# Design of Slosh-Free Robot Trajectories for Point-to-Point Motions Involving Both Position and Orientation

Simone Soprani[1], Roberto Di Leva[2], Gianluca Palli[1], Marco Carricato[2] and Luigi Biagiotti[3]

***Abstract*—Many research papers address the problem of optimizing robot trajectories for liquid transportation to prevent sloshing in highly dynamic motions. The approaches used may vary, but to the best of our knowledge, all these works share a common feature: only the desired position trajectory is considered as input, while the orientation of the end-effector is automatically computed to compensate for lateral acceleration. In this paper, we take a step forward toward real robotic applications by considering not only the position but also the orientation of the container about the vertical direction, which is a fundamental requirement for many pick-and-place tasks. Specifically, we assume that the position trajectory and the orientation about the $z$-axis are predefined, while the orientation about the $x$ and $y$-axes can be freely adjusted during motion to compensate for lateral accelerations. Through analytical considerations based on the sloshing model and experimental tests with a single container, we demonstrate that tilting compensation can be effective even when imposed rotational motions are present, provided that these motions are accounted for in the compensation strategy. Notably, this compensation action is computed in an analytical form, which, in principle, leads to a complete suppression of sloshing without the need for an optimization procedure. This makes the method computationally efficient and suitable for real-time implementation.**

***Index Terms*—Trajectory planning, Sloshing, Tilting compensation, Pick&place-like trajectories**

## I. Introduction

The manipulation of liquid-filled containers presents significant challenges in robotics, particularly when it comes to controlling sloshing behavior during dynamic motions. Sloshing, the unintended movement of liquid within a container, can have detrimental effects in a wide range of industrial applications. These include sectors such as aerospace, automotive, logistics, and packaging, where the containment and safe transport of liquids is critical. Specifically, in packaging and production lines, managing the movement of liquids within containers is essential for ensuring that products remain intact and without leakage. In these scenarios, the prevention of spillage, while maintaining high efficiency in motion and transport, is a key concern. Effective control of sloshing is therefore essential, especially in tasks such as pick-and-place operations, where the container is subjected to complex motions, including rotations and translations (Fig. 1).

Recent advancements in anti-sloshing control strategies have made significant steps in mitigating the effects of liquid motion during container manipulation. However, the control methods primarily focus on compensating for sloshing during simple motion trajectories. One critical aspect that has yet to be fully addressed is the impact of rotational motions, particularly about the $z$-axis, which can induce changes in the liquid behavior and in the consequent control strategy to be employed. This paper aims to extend existing anti-sloshing control techniques to the more complex task of pick-and-place operations. Specifically, we focus on the rotational dynamics around the $z$-axis, exploring how to incorporate rotation about this axis into the control algorithm, ensuring that the liquid behavior is managed effectively during these more intricate maneuvers.

## II. Related Works

The control of sloshing in liquid-filled containers has been the subject of extensive research due to its critical role in various industrial applications. Numerous strategies have been developed to mitigate sloshing, with a significant portion relying on model-based control approaches that utilize discrete mechanical approximations to capture the dynamic behavior of the liquid during motion. Among these, the two most widely adopted models are the mass-spring-damper system and the pendulum model. While trajectory optimization techniques based on mass-spring-damper models have shown promising results [1], [2], the pendulum model remains the predominant choice for control applications due to its ease of interpretation and effectiveness in capturing sloshing dynamics.

This work has been partially supported by the project PRIN 2020 "Co-Mir: Extending Robotic Manipulation Capabilities by Cooperative Mobile and Flexible Multi-Robot Systems", prot. 2020CMEFPK, and by the project "MATRIX: Robotic Manipulation and Transport of Liquids for High-Performance Industrial Applications."

[1]The authors are with the Department of Electrical, Electronic, and Information Engineering Guglielmo Marconi of the University of Bologna, Italy [simone.soprani2, gianluca.palli]@unibo.it.

[2] The authors are with the Department of Industrial Engineering of the University of Bologna, Italy [roberto.dileva, marco.carricato]@unibo.it.

[3]The author is with the engineering department Enzo Ferrari of the University of Modena and Reggio Emilia, Italy luigi.biagiotti@unimore.it.

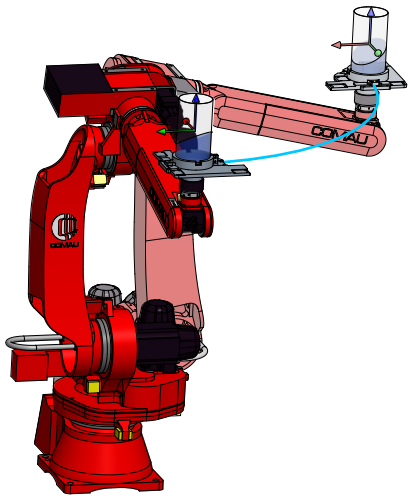

Figure 1: Point-to-point Motion with modification of the container orientation.

| Ref. | Motion dimensionality | | | | Control approach | | Implementation | |
|---|---|---|---|---|---|---|---|---|
| | 1 | 2 | 3 | 4 | Feed-forward | Feedback | Offline | Online |
| [2] | ✓ | ✓ | | | ✓ | | ✓ | |
| [3] | ✓ | | | | ✓ | | | ✓ |
| [4] | ✓ | | | | ✓ | | | ✓ |
| [5] | ✓ | ✓ | ✓ | | ✓ | | | ✓ |
| [7] | ✓ | | | | ✓ | | | ✓ |
| [8] | ✓ | | | | ✓ | | | ✓ |
| [11] | ✓ | | | | ✓ | | ✓ | |
| [12] | ✓ | ✓ | ✓ | | ✓ | | ✓ | |
| [13] | ✓ | ✓ | ✓ | | ✓ | | ✓ | |
| [14] | ✓ | ✓ | ✓ | | | ✓ | | ✓ |
| [20] | ✓ | | | | ✓ | | | ✓ |
| [22] | ✓ | ✓ | ✓ | | ✓ | | | ✓ |
| Our | ✓ | ✓ | ✓ | ✓ | ✓ | | | ✓ |

Table I: Main features of control methods for sloshing suppression in liquids transportation.

One of the primary challenges in sloshing control is the difficulty in obtaining real-time, and high-precision measurements of the liquid surface configuration. The implementation of sensor-based feedback control is often impractical, as the required measurement apparatus must achieve both high accuracy and minimal latency, which is not always feasible in industrial settings. As a result, feedforward control methods have emerged as a preferred approach, offering robust sloshing mitigation without the need for direct liquid state measurement. Early research in this field focused extensively on input shaping techniques, filtering methods, and smooth trajectory planning [3]–[6], which not only contributed to sloshing suppression but also facilitated online implementation, making these strategies well-suited for industrial applications.

In conjunction with these strategies, a widely adopted feedforward approach for sloshing control involves tilt compensation [7], [8]. In robotic applications, this method leverages the multi-degree-of-freedom capabilities of robotic manipulators to align the container's motion axis with the equivalent virtual pendulum. By minimizing relative motion between the liquid and the container, this technique effectively reduces sloshing while allowing for faster trajectory execution without compromising liquid stability or increasing the risk of spillage.

Another research direction focuses on trajectory optimization, where reference trajectories are computed based on the dynamic model of the system while incorporating constraints such as maximum velocity, acceleration, and obstacle avoidance [9]–[13]. While these optimization-based approaches typically yield time-efficient motion profiles, they are inherently limited to offline control, requiring the full trajectory to be predetermined and recalculated whenever modifications are needed. To mitigate this constraint, Model Predictive Control (MPC) strategies have recently been explored [14], enabling real-time trajectory adaptation while maintaining sloshing suppression.

Despite the advantages of feedforward control, such methods remain highly sensitive to unmodeled dynamics—particularly higher-order sloshing modes—and inaccuracies in system parameters. To enhance robustness, hybrid approaches that integrate feedforward and feedback control have been proposed [15]–[19], as well as employing multiple feedforward combined strategies incorporating input shaping with smoothing filters [20], [21] or tilt compensation [22]–[24]. Table I summarizes the main contributions of the cited papers, in terms of dimensionality of the considered motions, adopted control approaches and implementation capability.

However, most of the cited works primarily focus on translational motion, neglecting rotational dynamics, and often treat sloshing as an uncoupled phenomenon along independent axes. This simplification overlooks the intricate interactions that arise when rotations are introduced, particularly about the $z$-axis.

This paper aims to extend these previous contributions by addressing the combined effects of three-dimensional motion and vessel orientation. In particular, we focus on the impact of rotations about the $z$-axis, which have not been thoroughly investigated despite their influence on sloshing dynamics. By incorporating this additional degree of freedom into the control strategy, we aim to enhance the precision of sloshing mitigation in complex point-to-point motions, that are the basic elements for a practical applications, such as pick-and-place operations.

## III. 3D sloshing modeling of a liquid under Position and Orientation motions

Predicting the behavior of a liquid moving freely within a vessel is a complex challenge. While methods such as finite element analysis (FEM) [25] and computational fluid dynamics (CFD) [26] can model liquid dynamics, they are typically computationally intensive and unsuitable for model-based control strategies. A simpler and reasonably accurate alternative involves using discrete equivalent mechanical models, where the total liquid mass is represented by a mass rigidly attached to the container and several additional masses that oscillate relative to it, each representing a mode of oscillation of the liquid, capturing the sloshing effect. The two most commonly used models for representing liquid dynamics are the mass-spring-

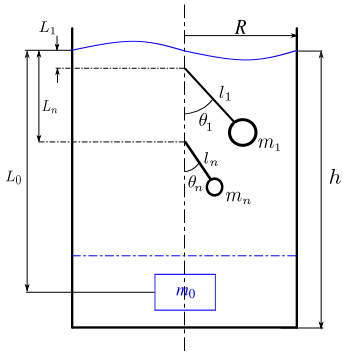


Figure 2: Equivalent mechanical model of the sloshing phenomenon using multiple pendulums.

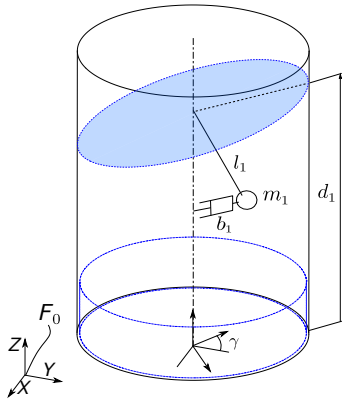


Figure 3: Spherical-pendulum model of the first sloshing mode in 3D space.

damper system and the pendulum system. While the mass-spring-damper model provides a reliable approximation of the liquid's behavior [27]–[29], the pendulum model is often preferred for control applications due to its simpler implementation and more intuitive representation of the liquid's motion. The pendulum model comprises a mass $m_0$ representing the portion of the liquid not involved in sloshing, positioned at a distance $L_0$ from the undisturbed liquid surface, and a series of pendulums representing the sloshing modes, each one of them with mass $m_n$ and length $l_n$, with pivots located at a distance $L_n$ from the static free surface of the liquid (see Fig. 2).

The parameters of the pendulum model can be determined by imposing equivalence conditions with the original continuum system [30]. In particular, the natural frequency of the $n$-th mode in the case of a cylindrical container of radius $R$ filled with a height $h$, is:

$$\omega_n = \sqrt{g\frac{\xi_{1n}}{R}\tanh\left(\xi_{1n}\frac{h}{R}\right)}, \tag{1}$$

where $\xi_{1n}$ is the root of the derivative of the Bessel function of the first kind [31], and $g$ is the gravity acceleration. The damping ratio $\zeta_n$ can be determined by using the experimental formula [30]:

$$\zeta_n = 0.92\sqrt{\frac{\upsilon/\rho}{\sqrt{gR^3}}}\left[1+\frac{0.318}{\sinh(\xi_{1n}h/R)}\left(1+\frac{1-h/R}{\cosh(\xi_{1n}h/R)}\right)\right] \tag{2}$$

From Eq.(1) it is possible to derive the length of the $n$-th pendulum by equating it to the natural frequency of a simple pendulum, given by $\sqrt{g/l_n}$:

$$l_n = \frac{R}{\xi_{1n}}\coth\left(\xi_{1n}\frac{h}{R}\right); \tag{3}$$

The vertical displacement of the $n$-th support point from the static liquid surface is given by [30]:

$$L_n = -\frac{2R}{\xi_{1n}\sinh(\xi_{1n}h/R)}. \tag{4}$$

For control applications, it is common practice to consider only the first asymmetric sloshing mode, as it is the most significant compared to higher-order modes [29]. Moreover, since the values of $L_n$ are typically small, they are often neglected in practical implementations. Different approaches exist to describe the spatial position of a generic pendulum mass using two angular variables. Hamaguchi et al. [32] [33] proposed a spherical pendulum model parametrized as a $y-x$ Euler angle rotation sequence. In contrast, Biagiotti et al. [6], [22], [23] employed a $z-y$ sequence, where the two angles, together with the pendulum rod length, define a spherical coordinate system. In this system, the first angle $\varphi$ defines the plane of sloshing, and the angle $\theta$ describes the sloshing motion. Although the $z-y$ parametrization exhibits a singularity at rest— when the pendulum aligns with the $z$-axis, any value of $\varphi$ corresponds to the same point—it offers a more intuitive geometric interpretation. While this parametrization may be unsuitable for accurately predicting sloshing height, its simplicity and ease of interpretation make it well-suited for control applications, it is therefore employed in this paper. The configuration of the pendulum mass is described by the generalized coordinates $\varphi$ and $\theta$, composed of the position of the pendulum pivot on top of the polar and azimuthal coordinates. Given a SCARA-like motion, where a 3D translation $[x,\, y,\, z]^T$ and a rotation $\gamma$ about the $z$-axis of the container are imposed (Fig. 3), it is possible to obtain the equations of motion of the spherical pendulum describing the behavior of the first sloshing mode through the energetic approach. The position vector $\boldsymbol{r}_1$ of the first sloshing mass becomes

$$\begin{aligned} {}^0\mathbf{r}_1 &= \begin{bmatrix} x \\ y \\ z \end{bmatrix} + \boldsymbol{R}_z(\gamma)\boldsymbol{R}_z(\varphi)\boldsymbol{R}_y(-\theta)\begin{bmatrix} 0 \\ 0 \\ -l_1 \end{bmatrix} = \\ &= \begin{bmatrix} x - l_1\sin\theta\,(\cos(\phi+\gamma)) \\ y + l_1\sin\theta\,(\sin(\phi+\gamma)) \\ z - l_1\cos\theta \end{bmatrix} \end{aligned} \tag{5}$$

with $\boldsymbol{R}_y$ and $\boldsymbol{R}_z$ representing the elementary rotation matrices about axes $y$ and $z$. The kinetic energy of mass $m_1$ is computed as

$$T = \frac{1}{2}m_1\left[\dot{x}_1^2 + \dot{y}_1^2 + \dot{z}_1^2\right] \tag{6}$$

with $x_1, y_1, z_1$ being the components of vector ${}^0r_1$, while the potential energy can be derived from

$$V = m_1 g z_1. \tag{7}$$

Finally the Rayleigh function $D$ accounts for energy dissipation.

$$D = \frac{1}{2} b_1 \left( \dot{x}_{r1}^2 + \dot{y}_{r1}^2 + \dot{z}_{r1}^2 \right) \tag{8}$$

where $[\dot{x}_{r1}\ \dot{y}_{r1}\ \dot{z}_{r1}]^T$ is the velocity of the pendulum mass relative to the container (obtained by setting $x, y, z$ and $\gamma$ identically equal to zero in Eq. (5)), and $b_1$ is the damping coefficient between the liquid and the container. Defining a generalized coordinate vector $\mathbf{q} = [q_1\ q_2]^T = [\varphi\ \theta]^T$, through the Lagrange equations

$$\frac{d}{dt}\left(\frac{\partial T}{\partial \dot{q}_i}\right) - \frac{\partial T}{\partial q_i} + \frac{\partial V}{\partial q_i} + \frac{\partial D}{\partial \dot{q}_i} = 0, \quad \text{for } i = 1, 2, \tag{9}$$

it is possible to obtain the equations of motion describing the dynamics of the spherical pendulum:

$$\begin{cases} \ddot{\theta} = -\frac{b_1}{m_1}\dot{\theta} - \frac{1}{l_1}\cos\theta\left(\cos(\gamma+\varphi)\ddot{x} + \sin(\gamma+\varphi)\ddot{y}\right) + \\ \qquad -\frac{1}{l_1}\cos\theta\left(\ddot{z}+g\right) + \cos\theta\sin\theta\left(\dot{\gamma}+\dot{\varphi}\right)^2 \\ \\ \ddot{\varphi}\sin\theta = -\frac{b_1}{m_1}\sin\theta\dot{\varphi} + \cos\theta\left(\dot{\gamma}+\dot{\varphi}\right)\dot{\theta} - \ddot{\gamma}\sin\theta + \\ \qquad +\frac{1}{l_1}\left(\sin(\gamma+\varphi)\ddot{x} - \cos(\gamma+\varphi)\ddot{y}\right) \end{cases} \tag{10}$$

From Eqs. (10), the steady-state configuration (by imposing the conditions $\dot{\theta} = \ddot{\theta} = \dot{\varphi} = \ddot{\varphi} = 0$) of the spherical pendulum is readily obtained by imposing that:

$$0 = \cos(\theta)\left(\cos(\gamma+\varphi)\ddot{x} + \sin(\gamma+\varphi)\ddot{y}\right) + \sin(\theta)(\ddot{z}+g) \tag{11a}$$

$$0 = \sin(\gamma+\varphi)\ddot{x} - \cos(\gamma+\varphi)\ddot{y} \tag{11b}$$

Isolating $\theta$ and $\varphi$ in Eqs. (11) gives:

$$\tan(\theta) = -\frac{\cos(\gamma+\varphi)\ddot{x} + \sin(\gamma+\varphi)\ddot{y}}{\ddot{z}+g} \tag{12a}$$

$$\tan(\gamma+\varphi) = \frac{\ddot{y}}{\ddot{x}} \tag{12b}$$

and thus

$$\varphi = -\gamma + \operatorname{atan2}(\ddot{y}, \ddot{x}) \tag{13a}$$

$$\theta = -\arctan\left(\frac{\sqrt{\ddot{x}^2+\ddot{y}^2}}{\ddot{z}+g}\right). \tag{13b}$$

## IV. Sloshing suppression based on tilting compensation

To implement a control strategy capable of counteracting pendulum oscillations, a feedforward control approach based on the dynamics of the spherical pendulum is adopted. Given the challenges associated with feedback control—primarily the need for fast and accurate sensors—a feedforward strategy is designed to mitigate and suppress pendulum oscillations by directly influencing the pendulum's dynamic equations.

While using filters to smooth the trajectory can effectively suppress sloshing dynamics once external excitations cease—provided that the natural frequency is accurately estimated—this approach only addresses the residual oscillations after the system stabilizes, without any control on the sloshing height during motion. However, to actively prevent sloshing during motion, it is necessary to align the vessel axis with the equivalent spherical pendulum. By ensuring that no relative movement occurs between the liquid and the container, the sloshing effect is minimized or entirely eliminated [23].

On the grounds of this, it is then reasonable to act on the vessel orientation by means of two angles, $\alpha$ and $\beta$, which are designed to align the vessel with the virtual pendulum. To implement the control strategy, these angles are applied to the vessel using a specific sequence of rotations. The orientation matrix $\boldsymbol{R}(\alpha, \beta)$ is constructed using the following $z-y-z$ rotation sequence:

$$\mathbf{R}(\alpha, \beta) = \mathbf{R}_z(\alpha)\mathbf{R}_y(\beta)\mathbf{R}_z(-\alpha), \tag{14}$$

where the role of each elementary rotation matrix is as follows:

- $\mathbf{R}_z(\alpha)$: a rotation about the $z$-axis by the angle $\alpha$ must align the vessel with the sloshing plane, therefore
$$\alpha = \varphi = -\gamma + \operatorname{atan2}(\ddot{y}, \ddot{x}).$$
- $\mathbf{R}_y(\beta)$: a rotation about the $y$-axis by the angle $\beta$ must adjust the pitch to counteract the pendulum motion, i.e.:
$$\beta = -\theta = \arctan\left(\frac{\sqrt{\ddot{x}^2+\ddot{y}^2}}{\ddot{z}+g}\right).$$
- $\mathbf{R}_z(-\alpha)$: a final rotation about the $z$-axis by the angle $-\alpha$ returns to the original reference frame.

The overall rotation matrix describing the orientation of the vessel becomes:

$$\mathbf{R}(\gamma, \alpha, \beta) = \mathbf{R}_z(\gamma)\mathbf{R}(\alpha, \beta), \tag{15}$$

where $\mathbf{R}_z(\gamma)$ represents the desired orientation about the $z$ axis, while $\mathbf{R}(\alpha, \beta)$ is the compensating orientation. Since the angles $\alpha$ and $\beta$ depend on the accelerations $\ddot{x}$, $\ddot{y}$ and $\ddot{z}$, in point-to-point motions, we have $\alpha = \beta = 0$ at the initial and final time instants, and therefore $\mathbf{R}(\alpha, \beta) = \boldsymbol{I}_3$. This means that the overall orientation will equal the desired pose, i.e., $\mathbf{R}(\gamma, \alpha, \beta) = \mathbf{R}_z(\gamma)$.

On the other hand, because of this dependency on $\ddot{x}$, $\ddot{y}$ and $\ddot{z}$, any discontinuities in these accelerations will cause abrupt changes in the vessel's orientation. Such sudden variations can result in undesired oscillations or overshooting, especially if the accelerations change rapidly or if the system response is not sufficiently fast to accommodate these changes. To ensure the continuity of the orientation angles, it is crucial that the acceleration profiles, along with the prescribed rotation $\gamma$, are at least $\mathbb{C}^1$ continuous. When these continuity conditions are satisfied, the feedforward control strategy can be effectively applied in both offline and online control contexts. In offline control, the system can pre-calculate the dynamics, enabling precise trajectory planning and orientation adjustments based on known acceleration profiles. In online control, the system

can respond in real-time to dynamic changes, ensuring smooth vessel movement and effectively mitigating sloshing effects.

### A. Center of rotation influence

The validity of this control strategy is inherently restricted to the scenario of a single object, where the center of rotation coincides with the center of mass of the pendulum. Under this condition, the control strategy can effectively suppress oscillations and align the vessel with the pendulum motion.

However, if a displacement were to be present between the center of rotation, where the tilting is applied, and the center of mass of the pendulum, the situation would become more complex. As the vessel tilts, centripetal forces arise, and these forces act on the pendulum center of mass, causing it to experience additional accelerations that are not accounted for in the original control model.

In this case, the tilting motion will generate centrifugal forces proportional to both the angular velocity and the angular acceleration of the vessel. These forces create a shift in the motion of the pendulum relative to the container, leading to a disparity between the actual and desired orientation. As a result, the control would likely fail to prevent or correct oscillations, reducing the overall performance and stability of the system.

To address these additional forces in systems with a displaced center of rotation, a more sophisticated control model would be necessary. This model would need to account for the centrifugal effects and adapt to the shifting dynamics.

This observation can be further substantiated by analyzing the equations of motion for a linear pendulum subjected to multiple external excitations, specifically lateral ($\ddot{x}$), vertical ($\ddot{z}$) and pitching ($\ddot{\beta}$) accelerations. These excitations introduce additional forces that modify the pendulum motion, and their effects can be understood by writing the corresponding dynamics equation. To do so, a similar method as the one used to obtain the equations of motion in Eqs. (10) is adopted, hence yielding:

$$\ddot{\theta} = -\frac{b_1}{m_1}\,\dot{\theta} - \frac{1}{l_1}\cos\left(\beta-\theta\right)\,\ddot{x} + \frac{1}{l_1}\sin\left(\beta-\theta\right)\,\left(\ddot{z}+g\right) + \\ + \frac{d_1}{l_1}\sin(\theta)\,\dot{\beta}^2 - \frac{1}{l_1}\left(l_1 - d_1\cos(\theta)\right)\,\ddot{\beta} \tag{16}$$

As observed, setting the displacement between the center of rotation and the pivot of the pendulum, $d_1$, equal to the length of the pendulum rod, $l_1$, effectively centers the rotation at the pendulum's mass. Under the assumption of no sloshing ($\theta = 0$), this configuration results in the complete cancellation of the terms that involve $\dot{\beta}^2$ and $\ddot{\beta}$. This effectively nullifies the additional forces arising from the tilting dynamics [24]. However, when this condition is not satisfied, these additional contributions become significant and reduce the effectiveness of the control strategy. Generally, since $\beta$ corresponds to the angle $\theta$ derived in Eq.(13b), its derivatives are directly influenced by changes in the accelerations. As the rate of change of the accelerations increases, the corresponding derivative of $\beta$ also grows, amplifying the impact of these dynamic effects. While the control approach can still mitigate sloshing to some extent, maintaining the same level of performance cannot be guaranteed under these conditions.

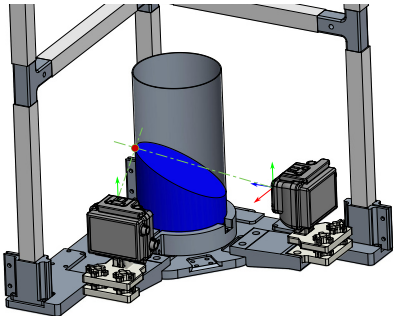

Figure 4: Mechanical structure of the experimental setup for sloshing detection through image processing analysis.

## V. Experimental results

To validate the capability of the control algorithm, experiments were conducted using a cylindrical container with a radius of $R = 49$ mm, filled with water up to a height of $h = 78$ mm. The trajectories were executed by a Comau Smart5 Six anthropomorphic robot.

To detect the sloshing height during motion, two GoPro Hero8 cameras were mounted on the flange of the robot, positioned with a 90° angular offset. The relative pose of the cameras was determined using an Aruco marker, and synchronization of the two video feeds was accomplished by cross-correlating the audio signals from each camera. For each camera, the coordinates of the detected peak were transformed from the image plane into 3D space and triangulated to obtain a unique point in the 3D space (see Figure 4).

The validity of the control was tested against three main types of prescribed motion:

- a straight-line translation with a $180^o$ rotation about the $z$-axis;
- a planar pick-and-place-type motion in which a $90^o$ rotation about the $y$-axis was imposed during the movement. Specifically, the $x$-axis of the tool was maintained tangent to the curve.
- a three-dimensional extension of the pick-and-place type motion, where an additional vertical motion is present.

To generate the trajectory, Finite Impulse Response (FIR) filters were employed. By using a cascade of these filters, a minimum-time multi-segment polynomial trajectory can be created, offering flexibility in adjusting the smoothness order and enabling the implementation of frequency-domain specifications and constraints on the maximum values of the position derivatives [34]. After estimating the natural frequency of the first vibration mode of the liquid used in the experiment, trajectories of class $\mathbb{C}^3$

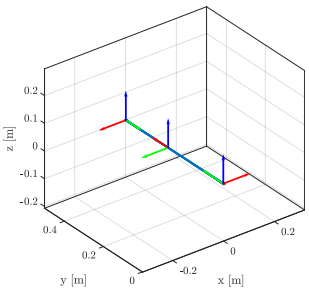


(a) Linear path.

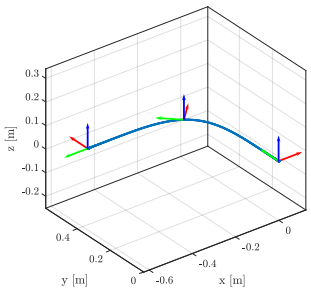


(b) Planar pick-and-place path.

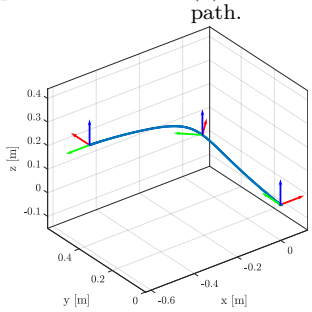


(c) 3D pick-and-place path.

Figure 5: Geometric paths considered in the experimental tests.

| $T_e$ | $\|\ddot{\mathbf{r}}\|_{max}$ | $\ddot{\theta}_{max}$ | $\overline{\eta}_{max-NC}$ | $\overline{\eta}_{max-C}$ |
|---|---|---|---|---|
| 1.36s | 3.9m/s$^2$ | 9.0rad/s$^2$ | 12.1mm | 2.8mm |
| 1.54s | 2.5m/s$^2$ | 7.1rad/s$^2$ | 10.6mm | 1.4mm |
| 1.62s | 1.7m/s$^2$ | 6.4rad/s$^2$ | 8.3mm | 1.1mm |
| 1.71s | 1.5m/s$^2$ | 5.8rad/s$^2$ | 7.2mm | 1.6mm |

Table II: Experimental results for the straight-line motion with different durations.

were generated. This approach successfully suppressed the residual vibrations at the primary vibration frequency.

### *A. Straight-line translation and z-axis rotation*

The first tested trajectory consists of a linear displacement combined with a 180$^o$ rotation about the container axis, governed by a smoothed trapezoidal motion law. The translation spans 0.5m and follows a smooth acceleration profile, leveraging the properties of the FIR cascade to ensure continuity.

The natural frequency of the system is estimated and actively suppressed, whereas the length of the virtual pendulum is computed using the relation $l_1 = g/w_1^2$. Table II presents the same trajectory executed under different dynamic conditions, with the last two columns reporting the maximum sloshing height reached without and with tilting compensation, respectively. Figures 6a and 7a illustrate the measured sloshing height for the most dynamic motion in both scenarios, where the red-highlighted section corresponds to the motion phase. The results indicate that tilting compensation reduces the total sloshing height by 75% during motion. Additionally, at the end of the trajectory, the FIR filters effectively suppress residual oscillations in both cases.

To further illustrate the compensation effect, Figures 6b and 7b display the force readings from a force-torque

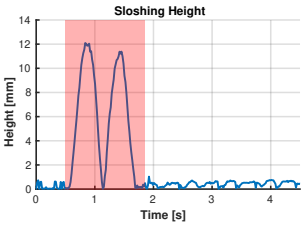


(a) Sloshing Height.

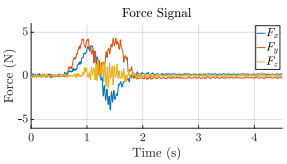


(b) Force Readings.

Figure 6: Experimental results with uncompensated straight-line motion.

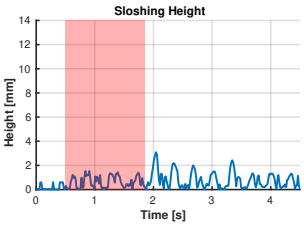


(a) Sloshing Height.

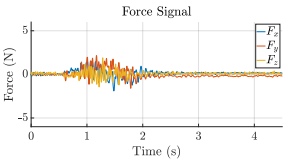


(b) Force Readings.

Figure 7: Experimental results with compensated straight-line motion.

sensor mounted on the robot flange. Similar to the liquid height measurements, these readings confirm that lateral excitations acting on the liquid-filled container are significantly reduced when compensation is applied.

In Figures 8a and 8b, snapshots of the liquid heights during uncompensated motion are shown, while Figures 9a and 9b present the corresponding compensated cases. The red and yellow dots represent the projection of the computed 3D point and the peak detected in the image plane, respectively. The minimal projection error, evident from the close overlap of the two markers, confirms the accuracy of the measurement.

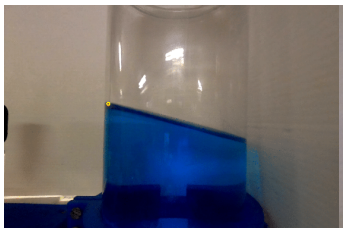

(a) Right view.

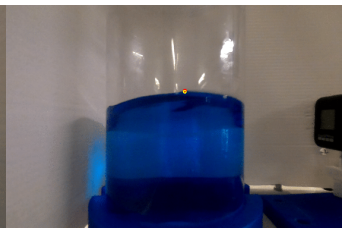

(b) Left view.

Figure 8: Camera views of uncompensated straight-line motion.

| $T_e$ | $\|\ddot{\mathbf{r}}\|_{max}$ | $\ddot{\theta}_{max}$ | $\overline{\eta}_{max-NC}$ | $\overline{\eta}_{max-C}$ |
|---|---|---|---|---|
| 1.93s | 3.5m/s$^2$ | 21.5rad/s$^2$ | 13.5mm | 4.2mm |
| 2.15s | 2.7m/s$^2$ | 16.3rad/s$^2$ | 9.7mm | 2.4mm |
| 2.33s | 2.4m/s$^2$ | 14.6rad/s$^2$ | 8.4mm | 1.6mm |
| 2.40s | 2.2m/s$^2$ | 13.1rad/s$^2$ | 7.5mm | 1.6mm |

Table III: Experimental results for the planar motion with different durations.

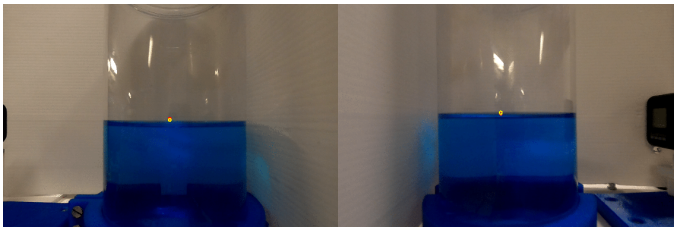

(a) Right view. (b) Left view.

Figure 9: Camera views of compensated straight-line motion.

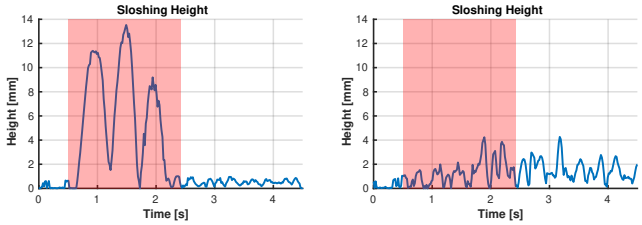


(a) Uncompensated Sloshing(b) Compensated Sloshing Height. Height.

Figure 10: Experimental results with planar motion.

### B. Planar trajectory and z-axis rotation

The second tested trajectory is designed to replicate typical pick-and-place operations. The geometric path followed by the container is depicted in Figure 5b, where a smooth, rounded trajectory is executed in conjunction with a $90^o$ rotation about the container axis.

As observed in Section V-A, the application of tilting compensation leads to a significant reduction in sloshing height during motion. This effect is clearly illustrated in Figures 10a and 10b, which compare the uncompensated and compensated cases for the most dynamic motion scenario. From Table III, we can see that the compensation leads to a reduction of the maximum sloshing height of at least 68%.

Similarly to the case of the straight-line translation and $z$-axis rotation, the oscillations of the liquid free surface are significantly reduced during motion. However, it is important to note that this control strategy remains effective only as long as the liquid surface remains planar. In highly dynamic motions, this assumption may no longer hold, as higher-order oscillation modes become more significant. Under such conditions, the liquid surface may deviate from planarity and take on the shape of a Bessel function, as described in [29].

### C. Three-dimensional translation and z-axis rotation

Finally, a three-dimensional trajectory was tested by extending the planar path from Section V-B with a 0.25m displacement along the $z$-axis while maintaining a 90° rotation about the same axis. Similar to the results in Sections V-A and V-B, the compensatory orientation adjustment effectively reduces sloshing height during motion. In Table IV, the results for different motion dynamics are presented. The data on maximum sloshing height clearly

| $T_e$ | $\|\ddot{\mathbf{r}}\|_{max}$ | $\dot{\theta}_{max}$ | $\overline{\eta}_{max-NC}$ | $\overline{\eta}_{max-C}$ |
|---|---|---|---|---|
| 1.93s | $3.7\text{m/s}^2$ | $21.5\text{rad/s}^2$ | 13.6mm | 3.3mm |
| 2.15s | $2.8\text{m/s}^2$ | $16.3\text{rad/s}^2$ | 8.7mm | 2.6mm |
| 2.33s | $2.5\text{m/s}^2$ | $14.6\text{rad/s}^2$ | 9.8mm | 2.1mm |
| 2.40s | $2.3\text{m/s}^2$ | $13.1\text{rad/s}^2$ | 7.5mm | 1.9mm |

Table IV: Experimental results for the 3D motion with different durations.

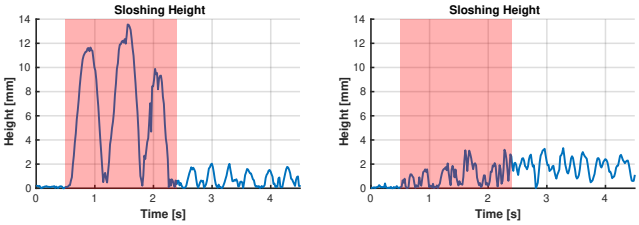


(a) Uncompensated Sloshing(b) Compensated Sloshing Height. Height.

Figure 11: Experimental results with 3D motion.

demonstrate that tilting compensation ensures a sloshing reduction of at least 70%. In Figures 11a and 11b the sloshing height comparison for the most dynamic motion is shown.

## VI. Conclusions

This paper extends feedforward sloshing control strategies to the complex task of pick-and-place operations involving liquid-filled containers. By incorporating rotational dynamics—specifically, rotations about the $z$-axis—into the control framework, we address a critical aspect of sloshing mitigation that has been largely overlooked in previous studies. Experimental validation demonstrated that the proposed approach effectively reduces sloshing height during motion, while the use of FIR filters ensures the suppression of residual oscillations at the end of the trajectory.

The proposed strategy assumes the center of rotation aligns with a single container's center of mass, enabling effective sloshing compensation. However, with multiple containers, varying rotational effects make this assumption invalid. Future work will focus on extending the control framework to handle multi-container manipulation while maintaining effective slosh suppression.

## References

[1] L. Guagliumi, A. Berti, E. Monti, and M. Carricato, "Anti-sloshing trajectories for high-acceleration motions in automatic machines," *Journal of Dynamic Systems, Measurement and Control, Transactions of the ASME*, vol. 144, 2022, prescribed motion, msd, filters,.

[2] R. D. Leva, M. Carricato, H. Gattringer, and A. Muller, "Time-optimal trajectory planning for anti-sloshing 2-dimensional motions of an industrial robot," in *2021 20th International Conference on Advanced Robotics, ICAR 2021*. Institute of Electrical and Electronics Engineers Inc., 2021, pp. 32–37, 2D msd optimization.

[3] A. Aboel-Hassan, M. Arafa, and A. Nassef, "Design and optimization of input shapers for liquid slosh suppression," *Journal of Sound and Vibration*, vol. 320, pp. 1–15, 2 2009, input shaper, 1D, no tilt.

[4] B. Pridgen, K. Bai, and W. Singhose, "Shaping container motion for multimode and robust slosh suppression," *Journal of Spacecraft and Rockets*, vol. 50, pp. 440–448, 2013.

[5] W. Aribowo, T. Yamashita, and K. Terashima, "Integrated trajectory planning and sloshing suppression for three-dimensional motion of liquid container transfer robot arm," *Journal of Robotics*, vol. 2015, pp. 1–15, 2015, 3D, spherical pendulum, input shaping, no tilting. [Online]. Available: http://www.hindawi.com/journals/jr/2015/279460/

[6] L. Moriello, L. Biagiotti, C. Melchiorri, and A. Paoli, "Control of liquid handling robotic systems: A feed-forward approach to suppress sloshing," in *2017 IEEE International Conference on Robotics and Automation (ICRA)*. IEEE, 5 2017, pp. 4286–4291. [Online]. Available: http://ieeexplore.ieee.org/document/7989493/

[7] J. T. Feddema, C. R. Dohrmann, G. G. Parker, R. D. Robinett, V. J. Romero, and D. J. Schmitt, "Control for slosh-free motion of an open container," *IEEE Control Systems*, vol. 17, pp. 29–36, 1997, simple pendulum. [Online]. Available: https://www.researchgate.net/publication/3206497_Control_for_slosh-free_motion_of_an_open_container

[8] S. J. Chen, B. Hein, and H. Worn, "Using acceleration compensation to reduce liquid surface oscillation during a high speed transfer," *Proceedings - IEEE International Conference on Robotics and Automation*, pp. 2951–2956, 2007, no relative motion between container and liquid.

[9] K. Yano and K. Terashima, "Robust liquid container transfer control for complete sloshing suppression," *IEEE Transactions on Control Systems Technology*, vol. 9, pp. 483–493, 5 2001. [Online]. Available: http://ieeexplore.ieee.org/document/918901/

[10] ——, "Sloshing suppression control of liquid transfer systems considering a 3-d transfer path," *IEEE/ASME Transactions on Mechatronics*, vol. 10, pp. 8–16, 2 2005.

[11] L. Consolini, A. Costalunga, A. Piazzi, and M. Vezzosi, "Minimum-time feedforward control of an open liquid container," *IECON Proceedings (Industrial Electronics Conference)*, pp. 3592–3597, 2013, optimization.

[12] J. Reinhold, M. Amersdorfer, and T. Meurer, "A dynamic optimization approach for sloshing free transport of liquid filled containers using an industrial robot," in *2019 IEEE/RSJ International Conference on Intelligent Robots and Systems (IROS)*. IEEE, 11 2019, pp. 2336–2341. [Online]. Available: https://ieeexplore.ieee.org/document/8968144/

[13] R. I. Muchacho, R. Laha, L. F. Figueredo, and S. Haddadin, "A solution to slosh-free robot trajectory optimization," in *IEEE International Conference on Intelligent Robots and Systems*, vol. 2022-October. Institute of Electrical and Electronics Engineers Inc., 2022, pp. 223–230.

[14] F. W. Chen and F. L. Lian, "Fast replanning slosh-free trajectory for mobile manipulation using model predictive control," in *International Conference on Advanced Robotics and Intelligent Systems, ARIS*. Institute of Electrical and Electronics Engineers Inc., 2024.

[15] K. Terashima, M. Hamaguchi, and K. Yamaura, "Modeling and input shaping control of liquid vibration for an automatic pouring system," in *Proceedings of 35th IEEE Conference on Decision and Control*, vol. 4. IEEE, 1996, pp. 4844–4850. [Online]. Available: http://ieeexplore.ieee.org/document/577707/

[16] K. Terashima and K. Yano, "Sloshing analysis and suppression control of tilting-type automatic pouring machine," *Control Engineering Practice*, vol. 9, pp. 607–620, 6 2001. [Online]. Available: https://linkinghub.elsevier.com/retrieve/pii/S0967066101000235

[17] M. Reyhanoglu and J. R. Hervas, "Point-to-point liquid container transfer via a ppr robot with sloshing suppression," in *2012 American Control Conference (ACC)*. IEEE, 6 2012, pp. 5490–5494. [Online]. Available: http://ieeexplore.ieee.org/document/6314687/

[18] ——, "Partial-state feedback control design for liquid container transfer with sloshing suppression," in *IECON 2012 - 38th Annual Conference on IEEE Industrial Electronics Society*. IEEE, 10 2012, pp. 2389–2393. [Online]. Available: http://ieeexplore.ieee.org/document/6388703/

[19] ——, "Robotically controlled sloshing suppression in point-to-point liquid container transfer," *JVC/Journal of Vibration and Control*, vol. 19, pp. 2137–2144, 10 2013.

[20] Q. Zang, J. Huang, and Z. Liang, "Slosh suppression for infinite modes in a moving liquid container," *IEEE/ASME Transactions on Mechatronics*, vol. 20, pp. 217–225, 2015.

[21] R. Nakagawa, T. Yamashita, and R. Tasaki, "Motion control of liquid containers with slosh constraints during high-speed three-dimensional transfer," in *2023 8th International Conference on Control and Robotics Engineering, ICCRE 2023*. Institute of Electrical and Electronics Engineers Inc., 2023, pp. 194–197.

[22] L. Moriello, L. Biagiotti, C. Melchiorri, and A. Paoli, "Manipulating liquids with robots: A sloshing-free solution," *Control Engineering Practice*, vol. 78, pp. 129–141, 9 2018.

[23] L. Biagiotti, D. Chiaravalli, L. Moriello, and C. Melchiorri, "A plug-in feed-forward control for sloshing suppression in robotic teleoperation tasks," in *2018 IEEE/RSJ International Conference on Intelligent Robots and Systems (IROS)*. IEEE, 10 2018, pp. 5855–5860, 3D tilting. [Online]. Available: https://ieeexplore.ieee.org/document/8593962/

[24] L. Biagiotti, D. Chiaravalli, R. Zanella, and C. Melchiorri, "Optimal feed-forward control for robotic transportation of solid and liquid materials via nonprehensile grasp," 6 2023, 3D, tilting, non prensile. [Online]. Available: http://arxiv.org/abs/2306.14212

[25] S. S. Kolukula and P. Chellapandi, "Nonlinear Finite Element Analysis of Sloshing," *Advances in Numerical Analysis*, vol. 2013, pp. 1–10, 2013.

[26] M. Schörgenhumer and A. Eitzlmayr, "Modeling of Liquid Sloshing with Application in Robotics and Automation," *IFAC-PapersOnLine*, vol. 52, no. 15, pp. 253–258, 2019. [Online]. Available: https://www.sciencedirect.com/science/article/pii/S240589631931674X

[27] R. D. Leva, M. Carricato, H. Gattringer, and A. Müller, "Sloshing dynamics estimation for liquid-filled containers under 2-dimensional excitation," in *Proceedings of the ECCOMAS Thematic Conference on Multibody Dynamics*. Budapest University of Technology and Economics, 2021, pp. 80–89.

[28] ——, "Sloshing dynamics estimation for liquid-filled containers performing 3-dimensional motions: modeling and experimental validation," *Multibody System Dynamics*, vol. 56, pp. 153–171, 10 2022.

[29] L. Guagliumi, A. Berti, E. Monti, and M. Carricato, "A simple model-based method for sloshing estimation in liquid transfer in automatic machines," *IEEE Access*, vol. 9, pp. 129 347–129 357, 2021.

[30] R. A. Ibrahim, *Liquid Sloshing Dynamics*. Cambridge University Press, 5 2005. [Online]. Available: https://www.cambridge.org/core/product/identifier/9780511536656/type/book

[31] H. F. Bauer, "Tables of zeros of cross product bessel functions," *Mathematics of Computation*, vol. 18, p. 128, 1 1964.

[32] M. HAMAGUCHI and T. TANIGUCHI, "Transfer control and curved path design for cylindrical liquid container," *IFAC Proceedings Volumes*, vol. 35, pp. 79–84, 2002. [Online]. Available: https://linkinghub.elsevier.com/retrieve/pii/S147466701539902X

[33] M. Hamaguchi, Y. Yoshida, T. Kihara, and T. Taniguchi, "Path design and trace control of a wheeled mobile robot to damp liquid sloshing in a cylindrical container," in *IEEE International Conference Mechatronics and Automation, 2005*, vol. 4. IEEE, 2005, pp. 1959–1964. [Online]. Available: http://ieeexplore.ieee.org/document/1626862/

[34] L. Biagiotti and C. Melchiorri, "Fir filters for online trajectory planning with time- and frequency-domain specifications," *Control Engineering Practice*, vol. 20, pp. 1385–1399, 12 2012.